ChemComm

Accepted Manuscript

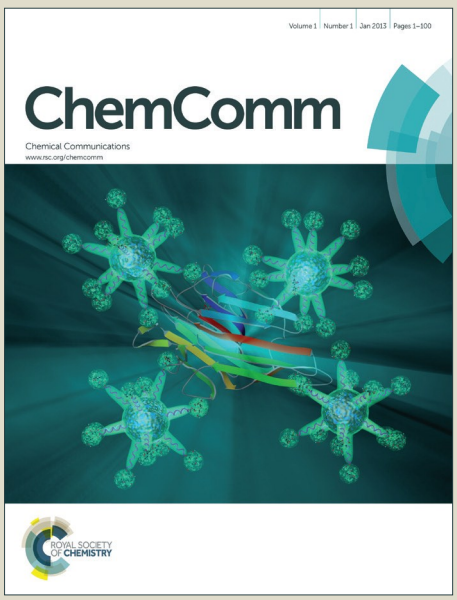

ROYAL SOCIETY OF CHEMISTRY

www.rsc.org/chemcomm

Journal Name

COMMUNICATION

L-Aspartate Links for Stable Sodium Metal-Organic Frameworks

Peter Siman,[a] Christopher A. Trickett,[a] Hiroyasu Furukawa[ab] and Omar M. Yaghi*[ab]

Received 00th January 20xx,
Accepted 00th January 20xx

DOI: 10.1039/x0xx00000x

www.rsc.org/

Metal-organic frameworks (MOFs) based purely on sodium are rare, typically due to large numbers of coordinating solvent ligands. We designed a tetratopic aspartate-based linker with flexible carboxylate groups to enhance framework stability. We report two new air-stable sodium MOFs, MOF-705 and MOF-706, comprising 2D sodium oxide sheets.

Metal-organic frameworks (MOFs) are extended porous structures in which multi-metallic secondary building units (SBUs) are joined by organic linkers.[1-5] Increasingly, MOFs with unusual thermal and chemical stability are being made, and investigated in many applications such as catalysis and gas storage.[6-10] MOFs based solely on sodium are few because of the tendency of sodium to coordinate a large ratio of solvent ligands to organic linkers, forming unstable frameworks with discrete or 1D sodium oxide building blocks that are highly sensitive to pore evacuation.[11-18] This instability is brought about by the loss of these solvent ligands, leading to structural collapse.[19] In this contribution, we show how the use of multiple carboxylate functionalities of L-aspartate to coordinate sodium gives two MOFs (Figure 1), MOF-705 [$Na_4(BDA)(CH_3OH)(H_2O)$], and the extended version MOF-706 [$Na_4(BPDA)(H_2O)_2$], in which the terminal ligands can be removed without collapse of their overall structure. We believe this is possible because of the ligand design of flexible L-aspartate carboxylates that facilitate the unique 2D sodium oxide secondary building units (SBUs) formation (Figure 1). This is supported by previous report using a similar link backbone but lacking the aspartate, which yielded a 1D SBU wherein the aspartate causes the polyhedra to share edges and/or corners to make the extended sheets.[12] These compounds represent the first examples of porous sodium MOFs which are air stable and retain their structure upon removal of guests even after a month at ambient conditions. The structures of both MOFs were determined by single crystal X-ray diffraction (SXRD) analysis, and further characterized by elemental analysis, NMR, and powder X-ray diffraction (PXRD). The gas adsorptive properties of these compounds indicate permanent porosity and their ability to uptake nitrogen and carbon dioxide.

The designed linkers H_4BDA (**1**) and H_4BPDA (**2**) (Figure 1a) were synthesized by coupling 1,4-benzenedicarboxylic acid (H_2BDC) or (1,1'-biphenyl)-4,4'-dicarboxylic acid (H_2BPDC) respectively, to the α-amine of L-aspartic acid (see Electronic Supporting Information (ESI), Section S1, for the detailed synthesis). MOF-705 was synthesized by the addition of H_4BDA to a methanolic solution of sodium hydroxide and heating to 50 °C while MOF-706 with H_4BPDA required heating to 70 °C (Section S2). The syntheses afforded needle-shaped colorless single crystals, with the dimensions of 0.01 × 0.01 × 0.05 mm^3 for MOF-705 and 0.005 × 0.005 × 0.03 mm^3 for MOF-706.

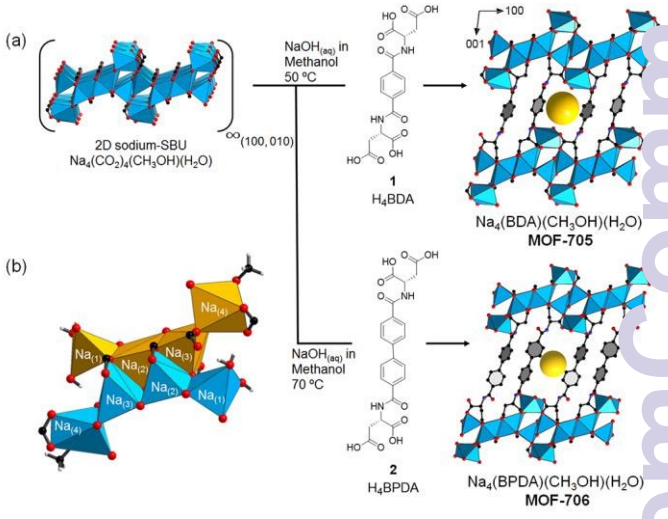

Figure 1. (a) Description of the crystal structures of 3D MOF-705 and MOF-706 made up of 2D sodium oxide sheets joined by organic linkers, H_4BDA and H_4BPDA respectively. (b) Two sets of the repeat unit ($Na_{(1)}$-$Na_{(4)}$) forming the sodium oxide sheets.

[a] Department of Chemistry, University of California - Berkeley, Materials Sciences Division, Lawrence Berkeley National Laboratory, and Kavli Energy NanoSciences Institute at Berkeley, Berkeley, California 94720, United States.
E-mail: yaghi@berkeley.edu
[b] King Fahd University of Petroleum and Minerals, Dhahran 34464, Saudi Arabia.
Electronic Supplementary Information (ESI) available: [details of any supplementary information available should be included here]. See DOI: 10.1039/x0xx00000x

In addition to single crystals, microcrystalline powder samples of these MOFs were obtained for higher yields by simply heating the reaction mixture to 85 °C, where the PXRD pattern of the microcrystalline product matched that simulated from the single crystal structure.

MOF-705 crystallizes in the chiral monoclinic $P2_1$ space group bearing the infinite 2D sodium oxide sheets extended in the [100] and [010] directions (Figure 1a and Table 1), with a repeat unit of four edge-sharing sodium atoms (Figure 1b). The first of these has square pyramidal geometry ($Na_{(1)}$), while the two in the middle are distorted trigonal bipyramids ($Na_{(2)}$ and $Na_{(3)}$), and the last is a distorted octahedron ($Na_{(4)}$). All the coordinating moieties are structural (an integral part of the MOF backbone) except for the octahedral $Na_{(4)}$, which is completed by the coordination of one methanol molecule. The $Na_{(1)}$ centers are bridged by two μ^2 water molecules in the [100] direction (Figure 1b), while μ^3 carboxylates connect all sodium atoms in the [010] direction. Completing the 3D structure, the linker joins these sodium oxide sheets in the [001] direction. The same applies for MOF-706, except that water molecules replace methanol coordinated to $Na_{(4)}$.

MOF-705 was immersed in a variety of organic solvents to explore the most suitable activation conditions (Figure S10). However, conventional methods to remove solvent from the pores were not successful causing both MOFs to collapse and form amorphous solids, so we turned to the use of supercritical CO_2 (SC-CO_2) activation from methanol. This yielded a crystalline material that was air stable for over a month in ambient conditions, as proven by PXRD and scanning electron microscopy (SEM, Figures 2 and S7). We observed by SXRD that methanol is still coordinated after this treatment, but can be removed to widen the pores by simply heating the SC-CO_2 activated sample at 70 °C under vacuum for 6 h. This evacuation of methanol guests was validated by thermogravimetric analysis (TGA) which showed no weight loss below 350 °C (Table S1 and Figure S12). Maximal surface area for MOF-706 can be achieved using SC-CO_2 from acetone, with no increase in surface area upon heating, unlike MOF-705 (Figure S11).

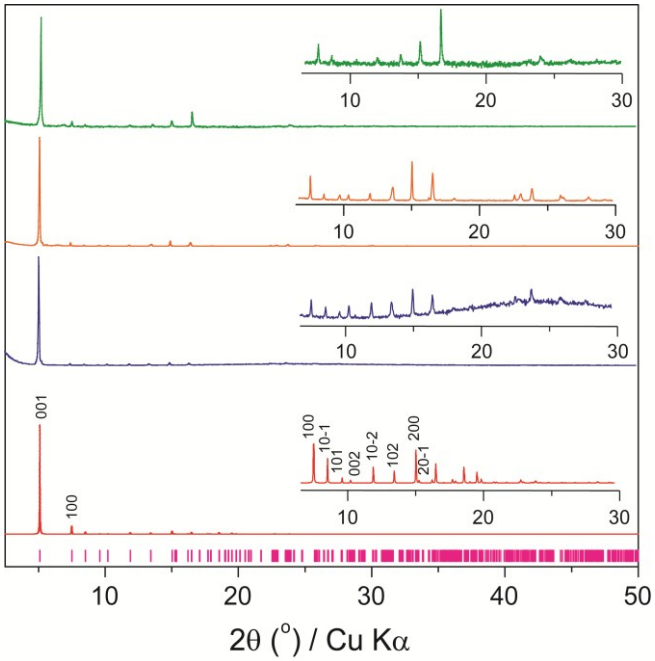

Figure 2. Observed reflection (purple) and PXRD patterns of MOF-705. Simulated from SXRD (red), as-synthesized (blue), SC-CO_2 activated (orange), heat activated (green).

Table 1. Crystallographic data of as-synthesized MOF-705 and MOF-706.

Sample[a]	MOF-705_as	MOF-706_a
Chemical Formula	$C_{17}H_{18}N_2Na_4O_{12}$	$C_{22.5}H_{18}N_2Na_4O_{12}$
Formula mass	534.29	618.87
Crystal system	monoclinic	monoclinic
Space group	$P2_1$	$P2_1$
λ [Å]	1.54178	0.88560
a [Å]	11.8894(4)	12.0790(15)
b [Å]	5.2299(2)	5.2419(6)
c [Å]	17.4663(5)	21.254(3)
β (degrees)	97.279(2)	103.886(6)
Z	2	2
V [Å^3]	1077.3(1)	1306.4(3)
T [K]	100(2)	100(2)
density [g cm^{-3}]	1.647	1.573
measured reflections	23262	7646
unique reflections	4415	1594
parameters	334	327
restraints	34	106
R_{int}	0.0889	0.1134
θ range (degrees)	2.55 - 74.52	2.164 - 21.724
R_1, wR_2	0.0415, 0.0965	0.0721, 0.209
S (GOF)	1.037	1.007
max / min res. dens. [e Å^{-3}]	0.366 / -0.241	0.535 / -0.45

[a] For the data of SC-CO_2 activated MOF-705 and MOF-706 please refer to the ESI, section S4.

The pores of SC-CO_2 activated MOF-705 were only accessible to CO_2 gas at 298 K (52 cm^3 cm^{-3}) while inaccessible for N_2 at 77 K (Figures S14 and S16). However the heat activated sample (following loss of the methanol) does uptake N_2 gas at 77 K, with a BET (Langmuir)surface area of 132 (231) m^2 g^{-1} (Figure S10) and with a steeper slope in the low pressure region of the CO_2 isotherm, indicating a strong gas framework interaction (Figure S16). On the other hand, despite the larger unit cell of MOF-706, the activated sample has a similar BET (Langmuir) surface area of 126 (216) m^2 g^{-1} and lower CO_2 uptake, probably due to guest molecules still coordinated to $Na_{(4)}$ (Figures S15 and S18).

The CO_2 uptake and slit-like pores of both MOFs led us to

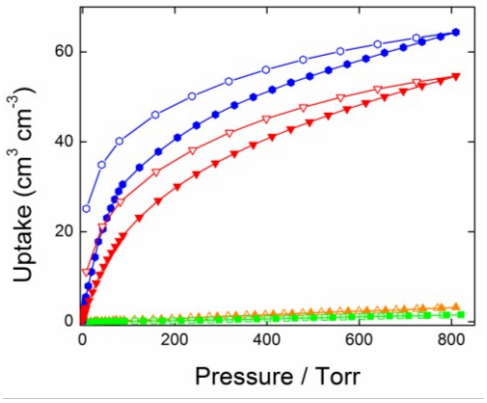

Figure 3. CO_2 and N_2 isotherms for MOF-705. N_2 isotherms are in orange (273 K) and green (298 K) while the CO_2 isotherms are in blue (273 K) and red (298 K). Filled and open symbols represent adsorption and desorption branches respectively. The connecting curves are guides for the eye.

test their selectivity towards CO_2 over N_2, with the objective of potentially employing these materials in CO_2 capture from post-combustion flue gas.[20-23] Indeed, we found good selectivity and affinity of the two MOFs for the CO_2 over N_2 at both 273 and 298 K (Figures 3, S18 and Table 2). The selectivity, of the MOFs which was assessed based on the uptake ratio of CO_2 over N_2 at different pressures, is high in comparison with other leading MOFs in this regard e.g. SIFSIX-2-Cu (13.7), ZIF-300 (22), Ni-MOF-74 (>10) and IRMOF-74-III (35),[17, 23-25] and is enhanced at the lower pressure region to reach 200 and 40 times, for MOF-705 and MOF-706 respectively, at 298 K and 80 Torr (Table 2).

In order for a material to be a successful candidate for an industrial application of gas separation, dynamic separation capacity of CO_2 over N_2 is desirable because CO_2 isotherms only show the thermodynamic capacity.[21-22, 27-28] To this end, breakthrough experiments were performed. A typical experiment involves passing a mixture of gases over the tested material to evaluate the selective capture of one gas, in this case CO_2, relative to the injection time compared to the other gases, specifically N_2. Performance is evaluated by the retention time; the longer the time needed for CO_2 to breakthrough (retention time), the higher the uptake and the better the separation capacity. Both MOFs were subjected to a binary gas mixture comprising 16% CO_2 and 84% N_2 (*v*/*v*). The breakthrough experiments (Figures 4, S19 and S20) showed that CO_2 breakthrough was delayed and that the MOFs successfully captured CO_2 in the presence of N_2. Moreover, the

Table 2. The crystal density, Q_{st} for CO_2, thermodynamic CO_2 and N_2 uptake, CO_2/N_2 selectivity for activated MOF-705 and MOF-706.

MOF	Crystal density ($cm^3\ g^{-1}$)	Q_{st} for CO_2 (kJ mol^{-1})	CO_2 uptake[a] ($cm^3\ cm^{-3}$)	N_2 uptake[a] ($cm^3\ cm^{-3}$)	CO_2/N_2 selectivity[a]
705	1.76	23	65	3.1	21
706	1.44	22	39	1.9	21

[a] At 800 Torr and 273 K.

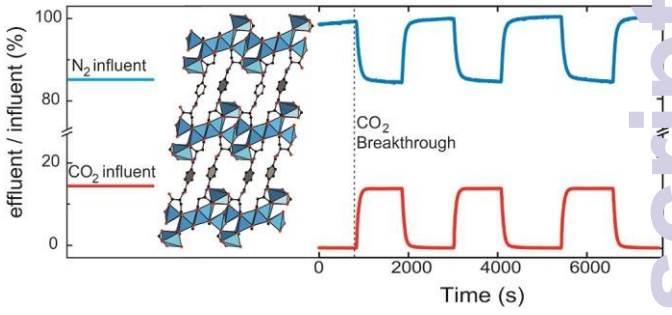

Figure 4. MOF-705 breakthrough cycles under dry conditions.

capture of CO_2 was efficient as more than 98% of the inlet CO_2 was captured (i.e. delayed breakthrough time), while N_2 gas passed through without interacting with the framework. Based on the breakthrough time, the uptake of MOF-705 was greater than MOF-706, 53 compared to 29 cm^3 [illegible] respectively, which is in agreement with the capacity displayed by CO_2 sorption measurements of 58 vs. 35 $cm^3\ cm^{-3}$. Finally, the regeneration of any material for CO_2 separation is an indispensable property, and both MOFs showed that they can be purged of CO_2 simply by flowing pure N_2 at ambient temperature. Within five minutes, 99.5% of adsorbed CO_2 was expelled from the framework. This method of desorption was effective over at least three cycles (Figure 4), confirming the very promising properties of this material for flue gas separation.

In summary, we present two new sodium-based MOFs, MOF-705 and MOF-706, that comprise a stable 2D SBU of sodium oxide sheets. The design of the linkers proved to be crucial for the formation and stabilization of these MOFs by taking advantage of the flexible tetratopic aspartate ends. This is evidenced by previous reports of sodium MOFs with similar but rigid carboxylate linkers resulting in discrete and 1D rod SBUs.[11-19] The combination of an air stable SBU and compact nature of the pore makes them strong candidates for CO_2 separation applications.

In this work, the synthesis was funded by BASF SE (Ludwigshafen, Germany). Funding pertaining to the gas adsorption and breakthrough measurements was provided by the Center for Gas Separations Relevant to Clean Energy Technologies, and Energy Frontier Research Center (EFRC) funded by the U.S. Department of Energy (DOE), Office of Science, Office of Basic Energy Sciences, under award DE-SC0001015. Work performed at the Advanced Light Source (ALS) is supported by the Director, Office of Science, Office of Basic Energy Sciences, of the U.S. Department of Energy under contract No. DE-AC02–05CH11231. NMR measurements were performed at the Molecular Foundry as a user project, which was supported by the Office of Science, Office of Basic Energy Sciences, of the DOE under Contract No. DE-AC02-05CH11231. We acknowledge B. Rungtaweevoranit and Dr. K. Choi (Yaghi group) for their assistance with electron microscopy, and Dr. P. Urban and E. Kapustin (Yaghi group), Dr. K. Gagnon and Dr. S. Teat (ALS) for valuable feedback on the crystal structure.

refinements. P.S. gratefully acknowledges the Israel Ministry of Science and Technology for the financial support.

CCDC 1420344-1420347 contain the supplementary crystallographic data for this paper. These data can be obtained free of charge from The Cambridge Crystallographic Data Centre.

Notes and references

1 H. C. Zhou and S. Kitagawa, *Chem. Soc. Rev.*, 2014, **43**, 5415-5418.
2 H. Furukawa, K. E. Cordova, M. O'Keeffe and O. M. Yaghi, *Science*, 2013, **341**, 974.
3 M. W. Hosseini, *Acc. Chem. Res.*, 2005, **38**, 313-323.
4 J. Rabone, Y. F. Yue, S. Y. Chong, K. C. Stylianou, J. Bacsa, D. Bradshaw, G. R. Darling, N. G. Berry, Y. Z. Khimyak, A. Y. Ganin, P. Wiper, J. B. Claridge and M. J. Rosseinsky, *Science*, 2010, **329**, 1053-1057.
5 H. Li, M. Eddaoudi, M. O'Keeffe and O. M. Yaghi, *Nature*, 1999, **402**, 276-279.
6 W. Lu, Z. Wei, Z. Y. Gu, T. F. Liu, J. Park, J. Park, J. Tian, M. Zhang, Q. Zhang, T. Gentle Iii, M. Bosch and H. C. Zhou, *Chem. Soc. Rev.*, 2014, **43**, 5561-5593.
7 C. Wang, D. Liu and W. Lin, *J. Am. Chem. Soc.*, 2013, **135**, 13222-13234.
8 M. O'Keeffe and O. M. Yaghi, *Chem. Rev.*, 2012, **112**, 675-702.
9 M. Eddaoudi, D. B. Moler, H. Li, B. Chen, T. M. Reineke, M. O'Keeffe and O. M. Yaghi, *Acc. Chem. Res.*, 2001, **34**, 319-330.
10 D. J. Tranchemontagne, J. L. Mendoza-Cortes, M. O'Keeffe and O. M. Yaghi, *Chem. Soc. Rev.*, 2009, **38**, 1257-1283.
11 P. Thuery, *CrystEngComm*, 2014, **16**, 1724-1734.
12 A. Choi, Y. K. Kim, T. K. Kim, M.-S. Kwon, K. T. Lee and H. R. Moon, *J. Mater. Chem. A*, 2014, **2**, 14986-14993.
13 D. S. Raja, J. H. Luo, C. T. Yeh, Y. C. Jiang, K. F. Hsu and C. H. Lin, *CrystEngComm*, 2014, **16**, 1985-1994.
14 D. L. Yang, X. Zhang, J. X. Yang, Y. G. Yao and J. Zhang, *Inorg. Chim. Acta*, 2014, **423**, 62-71.
15 D. S. Raja, J. H. Luo, C. Y. Wu, Y. J. Cheng, C. T. Yeh, Y. T. Chen, S. H. Lo, Y. L. Lai and C. H. Lin, *Cryst. Growth Des.*, 2013, **13**, 3785-3793.
16 D. L. Reger, A. Leitner, M. D. Smith, T. T. Tran and P. S. Halasyamani, *Inorg. Chem.*, 2013, **52**, 10041-10051.
17 S. Tominaka, S. Henke and A. K. Cheetham, *CrystEngComm*, 2013, **15**, 9400-9407.
18 Y. Liu, Z. U. Wang and H. C. Zhou, *Greenhouse. Gas. Sci. Technol.*, 2012, **2**, 239-259.
19 D. Banerjee and J. B. Parise, *Cryst. Growth Des.*, 2011, **11**, 4704-4720.
20 D. Li, H. Furukawa, H. X. Deng, C. Liu, O. M. Yaghi and D. S. Eisenberg, *Proc. Natl. Acad. Sci. U.S.A.*, 2014, **111**, 191-196.
21 A. M. Fracaroli, H. Furukawa, M. Suzuki, M. Dodd, S. Okajima, F. Gándara, J. A. Reimer and O. M. Yaghi, *J. Am. Chem. Soc.*, 2014, **136**, 8863-8866.
22 N. T. T. Nguyen, H. Furukawa, F. Gandara, H. T. Nguyen, K. E. Cordova and O. M. Yaghi, *Angew. Chem. Int. Ed.*, 2014, **53**, 10645-10648.
23 J. Liu, P. K. Thallapally, B. P. McGrail, D. R. Brown and J. Liu, *Chem. Soc. Rev.*, 2012, **41**, 2308-2322.
24 X. Lv, L. Li, S. Tang, C. Wang and X. Zhao, *Chem. Commun.*, 2014, **50**, 6886-6889.
25 D. S. Zhang, Z. Chang, Y. F. Li, Z. Y. Jiang, Z.-H. Xuan, Y. H. Zhang, J. R. Li, Q. Chen, T. L. Hu and X. H. Bu, *Sci. Rep.*, 2013, **3**.
26 K. Sumida, D. L. Rogow, J. A. Mason, T. M. McDonald, E. D. Bloch, Z. R. Herm, T.-H. Bae and J. R. Long, *Chem. Rev.*, 2012 **112**, 724-781.